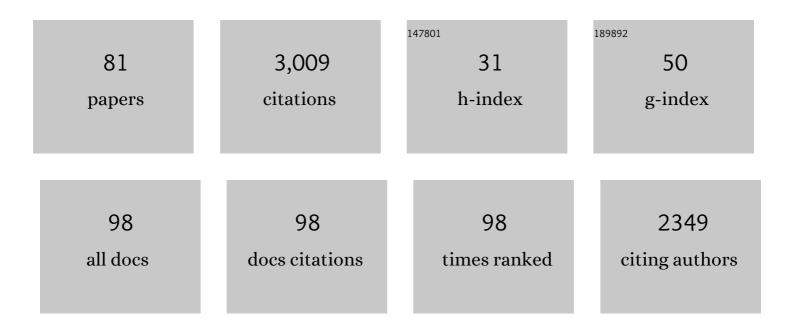
Noam Shemesh

List of Publications by Year in descending order

Source: https://exaly.com/author-pdf/804725/publications.pdf Version: 2024-02-01



#	Article	IF	CITATIONS
1	Correlation Tensor MRI deciphers underlying kurtosis sources in stroke. NeuroImage, 2022, 247, 118833.	4.2	15
2	Glucose fluxes in glycolytic and oxidative pathways detected in vivo by deuterium magnetic resonance spectroscopy reflect proliferation in mouse glioblastoma. NeuroImage: Clinical, 2022, 33, 102932.	2.7	14
3	Diffusion time dependence, power-law scaling, and exchange in gray matter. NeuroImage, 2022, 251, 118976.	4.2	34
4	Short <scp>TE</scp> downfield magnetic resonance spectroscopy in a mouse model of brain glioma. Magnetic Resonance in Medicine, 2022, 88, 524-536.	3.0	4
5	Soma and Neurite Density MRI (SANDI) of the in-vivo mouse brain and comparison with the Allen Brain Atlas. NeuroImage, 2022, 254, 119135.	4.2	9
6	In vivo Correlation Tensor MRI reveals microscopic kurtosis in the human brain on a clinical 3T scanner. Neurolmage, 2022, 254, 119137.	4.2	11
7	Stratification of radiosensitive brain metastases based on an actionable S100A9/RAGE resistance mechanism. Nature Medicine, 2022, 28, 752-765.	30.7	30
8	Double diffusion encoding and applications for biomedical imaging. Journal of Neuroscience Methods, 2021, 348, 108989.	2.5	27
9	Neuroplasticity-driven timing modulations revealed by ultrafast functional magnetic resonance imaging. Neurolmage, 2021, 225, 117446.	4.2	16
10	Beyond the diffusion standard model in fixed rat spinal cord with combined linear and planar encoding. NeuroImage, 2021, 231, 117849.	4.2	9
11	A rapid-onset diffusion functional MRI signal reflects neuromorphological coupling dynamics. Neurolmage, 2021, 231, 117862.	4.2	16
12	Effective bowel motion reduction in mouse abdominal MRI using hyoscine butylbromide. Magnetic Resonance in Medicine, 2021, 86, 2146-2155.	3.0	3
13	Evidence for microscopic kurtosis in neural tissue revealed by correlation tensor MRI. Magnetic Resonance in Medicine, 2021, 86, 3111-3130.	3.0	13
14	High temporal resolution functional magnetic resonance spectroscopy in the mouse upon visual stimulation. NeuroImage, 2021, 234, 117973.	4.2	11
15	On the generalizability of diffusion MRI signal representations across acquisition parameters, sequences and tissue types: Chronicles of the MEMENTO challenge. NeuroImage, 2021, 240, 118367.	4.2	10
16	Optogenetic activation of striatal D1R and D2R cells differentially engages downstream connected areas beyond the basal ganglia. Cell Reports, 2021, 37, 110161.	6.4	15
17	Validation and noise robustness assessment of microscopic anisotropy estimation with clinically feasible double diffusion encoding MRI. Magnetic Resonance in Medicine, 2020, 83, 1698-1710.	3.0	12
18	Higherâ€order diffusion MRI characterization of mesorectal lymph nodes in rectal cancer. Magnetic Resonance in Medicine, 2020, 84, 348-364.	3.0	8

NOAM SHEMESH

#	Article	lF	CITATIONS
19	Diffusion Kurtosis Imaging maps neural damage in the EAE model of multiple sclerosis. NeuroImage, 2020, 208, 116406.	4.2	19
20	High-Resolution 3D in vivo Brain Diffusion Tensor Imaging at Ultrahigh Fields: Following Maturation on Juvenile and Adult Mice. Frontiers in Neuroscience, 2020, 14, 590900.	2.8	8
21	Correlation tensor magnetic resonance imaging. NeuroImage, 2020, 211, 116605.	4.2	56
22	SANDI: A compartment-based model for non-invasive apparent soma and neurite imaging by diffusion MRI. NeuroImage, 2020, 215, 116835.	4.2	155
23	Noninvasive quantification of axon radii using diffusion MRI. ELife, 2020, 9, .	6.0	137
24	Measuring Microstructural Features Using Diffusion MRI. Advances in Magnetic Resonance Technology and Applications, 2020, , 571-604.	0.1	1
25	Effects of nongaussian diffusion on "isotropic diffusion―measurements: An ex-vivo microimaging and simulation study. Journal of Magnetic Resonance, 2019, 300, 84-94.	2.1	58
26	Evaluation of principal component analysis image denoising on multiâ€exponential MRI relaxometry. Magnetic Resonance in Medicine, 2019, 81, 3503-3514.	3.0	53
27	Short echo time relaxationâ€enhanced MR spectroscopy reveals broad downfield resonances. Magnetic Resonance in Medicine, 2019, 82, 1266-1277.	3.0	13
28	Susceptibility Perturbation MRI Maps Tumor Infiltration into Mesorectal Lymph Nodes. Cancer Research, 2019, 79, 2435-2444.	0.9	4
29	Microscopic anisotropy misestimation in sphericalâ€mean single diffusion encoding MRI. Magnetic Resonance in Medicine, 2019, 81, 3245-3261.	3.0	63
30	Layer-specific connectivity revealed by diffusion-weighted functional MRI in the rat thalamocortical pathway. NeuroImage, 2019, 184, 646-657.	4.2	33
31	BOLD-fMRI in the mouse auditory pathway. NeuroImage, 2018, 165, 265-277.	4.2	15
32	Incomplete initial nutation diffusion imaging: An ultrafast, singleâ€scan approach for diffusion mapping. Magnetic Resonance in Medicine, 2018, 79, 2198-2204.	3.0	5
33	Diffusion time dependence of microstructural parameters in fixed spinal cord. NeuroImage, 2018, 182, 329-342.	4.2	95
34	Insights into brain microstructure from in vivo DW-MRS. NeuroImage, 2018, 182, 97-116.	4.2	62
35	Two-dimensional magnetization-transfer – CPMG MRI reveals tract-specific signatures in fixed rat spinal cord. Journal of Magnetic Resonance, 2018, 297, 124-137.	2.1	4
36	Accurate estimation of microscopic diffusion anisotropy and its time dependence in the mouse brain. NeuroImage, 2018, 183, 934-949.	4.2	46

NOAM SHEMESH

#	Article	IF	CITATIONS
37	Axon Diameters and Myelin Content Modulate Microscopic Fractional Anisotropy at Short Diffusion Times in Fixed Rat Spinal Cord. Frontiers in Physics, 2018, 6, .	2.1	23
38	Transverse relaxation of selectively excited metabolites in stroke at 21.1 T. Magnetic Resonance in Medicine, 2017, 77, 520-528.	3.0	11
39	Efficient spectroscopic imaging by an optimized encoding of pretargeted resonances. Magnetic Resonance in Medicine, 2017, 77, 511-519.	3.0	1
40	White matter biomarkers from fast protocols using axially symmetric diffusion kurtosis imaging. NMR in Biomedicine, 2017, 30, e3741.	2.8	37
41	Mapping axonal density and average diameter using non-monotonic time-dependent gradient-echo MRI. Journal of Magnetic Resonance, 2017, 277, 117-130.	2.1	25
42	Measuring Microscopic Anisotropy with Diffusion Magnetic Resonance: From Material Science to Biomedical Imaging. Mathematics and Visualization, 2017, , 229-255.	0.6	1
43	Internal gradient distributions: A susceptibility-derived tensor delivering morphologies by magnetic resonance. Scientific Reports, 2017, 7, 3311.	3.3	12
44	Double oscillating diffusion encoding and sensitivity to microscopic anisotropy. Magnetic Resonance in Medicine, 2017, 78, 550-564.	3.0	26
45	Distinguishing neuronal from astrocytic subcellular microstructures using in vivo Double Diffusion Encoded 1H MRS at 21.1 T. PLoS ONE, 2017, 12, e0185232.	2.5	24
46	Conventions and nomenclature for double diffusion encoding NMR and MRI. Magnetic Resonance in Medicine, 2016, 75, 82-87.	3.0	154
47	Fast imaging of mean, axial and radial diffusion kurtosis. NeuroImage, 2016, 142, 381-393.	4.2	54
48	Size Distribution Imaging by Non-Uniform Oscillating-Gradient Spin Echo (NOGSE) MRI. PLoS ONE, 2015, 10, e0133201.	2.5	32
49	Diffusion-assisted selective dynamical recoupling: A new approach to measure background gradients in magnetic resonance. Journal of Chemical Physics, 2014, 140, 084205.	3.0	11
50	Metabolic properties in stroked rats revealed by relaxation-enhanced magnetic resonance spectroscopy at ultrahigh fields. Nature Communications, 2014, 5, 4958.	12.8	53
51	Metabolic T ₁ Dynamics and Longitudinal Relaxation Enhancement <i>In Vivo</i> at Ultrahigh Magnetic Fields on Ischemia. Journal of Cerebral Blood Flow and Metabolism, 2014, 34, 1810-1817.	4.3	10
52	Coherent Dynamical Recoupling of Diffusion-Driven Decoherence in Magnetic Resonance. Physical Review Letters, 2013, 111, 080404.	7.8	24
53	The CONNECT project: Combining macro- and micro-structure. NeuroImage, 2013, 80, 273-282.	4.2	121
54	Measuring small compartment dimensions by probing diffusion dynamics via Non-uniform Oscillating-Gradient Spin-Echo (NOGSE) NMR. Journal of Magnetic Resonance, 2013, 237, 49-62.	2.1	34

NOAM SHEMESH

#	Article	lF	CITATIONS
55	Diffusion weighted MRI by spatiotemporal encoding: Analytical description and in vivo validations. Journal of Magnetic Resonance, 2013, 232, 76-86.	2.1	44
56	Shemesh, Westin, and Cohen Reply:. Physical Review Letters, 2013, 110, 109802.	7.8	1
57	Longitudinal Relaxation Enhancement in ¹ Hâ€NMR Spectroscopy of Tissue Metabolites via Spectrally Selective Excitation. Chemistry - A European Journal, 2013, 19, 13002-13008.	3.3	25
58	Magnetic Resonance Imaging by Synergistic Diffusion-Diffraction Patterns. Physical Review Letters, 2012, 108, 058103.	7.8	36
59	Publisher's Note: Magnetic Resonance Imaging by Synergistic Diffusion-Diffraction Patterns [Phys. Rev. Lett. 108 , 058103 (2012)]. Physical Review Letters, 2012, 108, .	7.8	1
60	Mapping apparent eccentricity and residual ensemble anisotropy in the gray matter using angular double-pulsed-field-gradient MRI. Magnetic Resonance in Medicine, 2012, 68, spcone-spcone.	3.0	0
61	Mapping apparent eccentricity and residual ensemble anisotropy in the gray matter using angular doubleâ€pulsedâ€fieldâ€gradient MRI. Magnetic Resonance in Medicine, 2012, 68, 794-806.	3.0	41
62	Mesenchymal stem cells induced to secrete neurotrophic factors attenuate quinolinic acid toxicity: A potential therapy for Huntington's disease. Experimental Neurology, 2012, 234, 417-427.	4.1	69
63	Accurate noninvasive measurement of cell size and compartment shape anisotropy in yeast cells using doubleâ€pulsed field gradient MR. NMR in Biomedicine, 2012, 25, 236-246.	2.8	51
64	Probing Microscopic Architecture of Opaque Heterogeneous Systems Using Double-Pulsed-Field-Gradient NMR. Journal of the American Chemical Society, 2011, 133, 6028-6035.	13.7	50
65	Overcoming apparent Susceptibility-Induced Anisotropy (aSIA) by bipolar double-Pulsed-Field-Gradient NMR. Journal of Magnetic Resonance, 2011, 212, 362-369.	2.1	25
66	Microscopic and compartment shape anisotropies in gray and white matter revealed by angular bipolar double-PFG MR. Magnetic Resonance in Medicine, 2011, 65, 1216-1227.	3.0	67
67	Pore diameter mapping using double pulsed-field gradient MRI and its validation using a novel glass capillary array phantom. Journal of Magnetic Resonance, 2011, 208, 128-135.	2.1	70
68	Nuclear magnetic resonance characterization of general compartment size distributions. New Journal of Physics, 2011, 13, 015010.	2.9	31
69	Longitudinal MRI and MRSI characterization of the quinolinic acid rat model for excitotoxicity: peculiar apparent diffusion coefficients and recovery of Nâ€acetyl aspartate levels. NMR in Biomedicine, 2010, 23, 196-206.	2.8	9
70	From singleâ€pulsed field gradient to doubleâ€pulsed field gradient MR: gleaning new microstructural information and developing new forms of contrast in MRI. NMR in Biomedicine, 2010, 23, 757-780.	2.8	95
71	Late stimulation of the sphenopalatineâ€ganglion in ischemic rats: Improvement in Nâ€acetylâ€aspartate levels and diffusion weighted imaging characteristics as seen by MR. Journal of Magnetic Resonance Imaging, 2010, 31, 1355-1363.	3.4	23
72	Detecting diffusion-diffraction patterns in size distribution phantoms using double-pulsed field gradient NMR: Theory and experiments. Journal of Chemical Physics, 2010, 132, 034703.	3.0	65

#	Article	IF	CITATIONS
73	Noninvasive bipolar double-pulsed-field-gradient NMR reveals signatures for pore size and shape in polydisperse, randomly oriented, inhomogeneous porous media. Journal of Chemical Physics, 2010, 133, 044705.	3.0	71
74	A general framework to quantify the effect of restricted diffusion on the NMR signal with applications to double pulsed field gradient NMR experiments. Journal of Chemical Physics, 2009, 130, 104702.	3.0	93
75	Measuring small compartmental dimensions with low-q angular double-PGSE NMR: The effect of experimental parameters on signal decay. Journal of Magnetic Resonance, 2009, 198, 15-23.	2.1	62
76	Observation of restricted diffusion in the presence of a free diffusion compartment: Single- and double-PFG experiments. Journal of Magnetic Resonance, 2009, 200, 214-225.	2.1	36
77	Protective Effects of Neurotrophic Factor–Secreting Cells in a 6-OHDA Rat Model of Parkinson Disease. Stem Cells and Development, 2009, 18, 1179-1190.	2.1	136
78	Adult neurotrophic factor-secreting stem cells: a potential novel therapy for neurodegenerative diseases. Israel Medical Association Journal, 2009, 11, 201-4.	0.1	34
79	The effect of experimental parameters on the signal decay in double-PCSE experiments: Negative diffractions and enhancement of structural information. Journal of Magnetic Resonance, 2008, 195, 153-161.	2.1	28
80	Migration of Neurotrophic Factors-Secreting Mesenchymal Stem Cells Toward a Quinolinic Acid Lesion as Viewed by Magnetic Resonance Imaging. Stem Cells, 2008, 26, 2542-2551.	3.2	72
81	Optogenetic Activation of Striatal D1/D2 Medium Spiny Neurons Differentially Engages Downstream Connected Areas Beyond the Basal Ganglia. SSRN Electronic Journal, 0, , .	0.4	0